Investigation of the Dynamics of Microdevices – as a Design Tool

D. J. Seter*, O. Degani**, S. Kaldor*, E. Scher* and Y. Nemirovsky**

*RAFAEL – Mimcrosystems Group
POB 2250 Haifa 31201, Israel, danyz@rafael.co.il
**Kidron Microelectronics Research Center, Electrical Engineering Department,
Technion, Haifa 32000 Israel ofird@tx.technion.ac.il

ABSTRACT

When designing microaccelerometers, microgyroscopes and other microdevices, there is a strong need for dynamic understanding in system level. Thus, dynamic simulation is a part of many CAD tools for MEMS [1]. In this work, a relatively simple approach is presented for the study of the dynamics of microdevices. The theoretical derivation of the equations of motion is based on the Newton-Euler approach and provides a matrix form that is convenient to integrate. The dynamical model combined with models for electrostatic actuation and squeeze film effects [2] is verified by comparison with experimental results: the decaying motion of a microresonator due to an electrostatic impulse. Good agreement between simulation and measurements is shown. The pull-in angle and voltage are simulated and compared to theoretical calculations that were presented by the authors [3]. Finally, the model is used for parametric study of the influence of geometrical variations on the dynamics of a microgyroscope.

Keywords: Microgyroscopes, dynamics, simulations, squeeze-film, angular pull-in.

1 THE DYNAMICAL MODEL

The dynamical model refers to the microdevice as a general shaped rigid body of mass m and inertia I, as shown in Figure 1. The body is attached to a rigid frame via N_k elastic elements. Damping effects are modeled by N_d damping elements attached to the body. In this section the derivation of the dynamics is treated while the elastic and damping loads are addressed in section 2. Three Cartesian systems of coordinates are used: The inertial system is designated $\mathbf{e}^{\mathbf{O}}$, the frame system $\mathbf{e}^{\mathbf{F}}$ and the body fixed system $\mathbf{e}^{\mathbf{B}}$. The origin of $\mathbf{e}^{\mathbf{F}}$ and $\mathbf{e}^{\mathbf{B}}$ coincide with the center of mass of the frame and the body respectively. For the rigid body, under the action of $\mathbf{F}^{\mathbf{e}}$ – the external forces resultant and $\mathbf{T}^{\mathbf{e}}$ – the external moments resultant, two vector equations of motion can be written:

$$m\frac{d^2}{dt^2}r_{ocg} = F^e \qquad (1a)$$

$$\frac{d}{dt}H_m = T^e \qquad (1b)$$

Where r_{0cg} is the radius vector of the bodys' center of mass in respect to the inertial origin and H is the absolute angular momentum vector of the body. The motion of the frame is constrained (pre-prescribed) and thus its absolute linear velocity – $\mathbf{V}_\mathbf{F}$, absolute linear acceleration $\mathbf{a}_\mathbf{F}$, angular velocity $\Omega_\mathbf{F}$ and angular acceleration $\Gamma_\mathbf{F}$ are all known. The angular velocity and angular acceleration of body m relative to $\mathbf{e}^{\mathbf{F}}$, resolved in $\mathbf{e}^{\mathbf{m}}$, are designated $\omega^{\mathbf{m}}_{\mathbf{m}}$ and $\alpha^{\mathbf{m}}_{\mathbf{m}}$ respectively. By using the classic Euler-Angles [4], $\omega^{\mathbf{m}}_{\mathbf{m}}$ can be written as: $\underline{\mathbf{B}}_{\mathbf{Fm}}\,\lambda$ where λ is a column vector containing the first time derivatives of the rotation-angles and $\underline{\mathbf{B}}_{\mathbf{Fm}}$ is the appropriate transformation matrix. By time differentiation of $\omega^{\mathbf{F}}_{\mathbf{m}}$, $\alpha^{\mathbf{F}}_{\mathbf{m}}$ can be obtained. The absolute angular velocity of body m is designated $\Omega^{\mathbf{F}}\mathbf{m}$ and is given by $\Omega^{\mathbf{F}}_{\mathbf{F}}+\omega^{\mathbf{F}}_{\mathbf{m}}$ and the absolute angular acceleration of m is $\Gamma^{\mathbf{F}}_{\mathbf{m}}$ given by $\Gamma^{\mathbf{F}}_{\mathbf{F}} + \alpha^{\mathbf{F}}_{\mathbf{m}}$. $\Omega^{\mathbf{F}}_{\mathbf{F}}$ and $\Gamma^{\mathbf{F}}_{\mathbf{F}}$ are the absolute angular velocity and acceleration of the frame, respectively, resolved in $\mathbf{e}^{\mathbf{F}}$. In the present derivation, the vector product operator is replaced by the known tilde operator [5] to form a linear operation between two matrices $\underline{\mathbf{U}}$ and $\underline{\mathbf{V}}$:

$$\underline{U} \leftrightarrow \underline{V} = \underline{\tilde{U}}\,\underline{V} \qquad (2)$$

Referring to Figure 1: $\mathbf{r}_{\mathbf{ocg}} = \mathbf{r}_{\mathbf{oF}}+\mathbf{r}_{\mathbf{Fcg}}$. The absolute angular momentum vector is given by: $\mathbf{H}_\mathbf{m}=\underline{\mathbf{I}}\Omega_\mathbf{m}$. By substitution $\mathbf{r}_{\mathbf{ocg}}$ and $\underline{\mathbf{H}}_\mathbf{m}$ into equations (1a) and (1b) and differentiating in respect to time, the following two vector equations of motion are obtained, resolved in $\mathbf{e}^{\mathbf{F}}$:

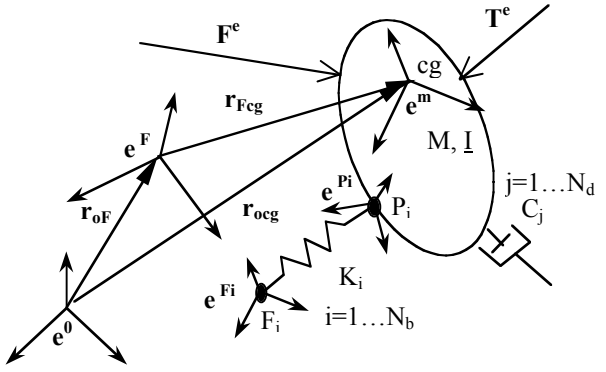

Figure 1: Systems of coordinates and vectors definition for the dynamical model.

$$a_F^F + \ddot{r}_{Fcg} + 2\tilde{\Omega}_F^F \dot{r}_{Fcg} + \tilde{\Gamma}_F^F r_{Fcg}^F = F^e \tag{3a}$$

$$\underline{\underline{A_{Fm} I B_{Fm}}}\dot{\lambda} + \underline{A}_{Fm}\left\{\left[\underline{A}_{Fm}\Gamma_F^F + \dot{\underline{B}}_{Fm}\lambda\right] + \left[\underline{A}_{mF}\Omega_F^F + \omega_m^F\right]\left(\underline{I}\left[\underline{A}_{mF}\Omega_F^F + \omega_m^F\right]\right)\right\} = T^e \tag{3b}$$

$\underline{\mathbf{A}}_{ij}$ is the transformation matrix used to resolve a vector $\mathbf{r}^j$ given in $\mathbf{e}^j$ in system $\mathbf{e}^i$. The underlined terms refer to column vectors containing the second time derivatives of the degrees of freedom. By rearranging Eqs. (3a) and (3b) a matrix form for the equations of motion is obtained:

$$\underline{A}\ddot{\underline{X}} = \underline{B} \tag{4}$$

$\underline{A}$ is a 6×6 square matrix. It's element are nonlinear functions of the degrees of freedom and inertial properties of the body. $\underline{B}$ is a 6×1 column vector. It's elements are nonlinear functions of: the degrees of freedom, their first time derivative, the inertial properties of the body and the external loads. $\underline{X}$ is a 6×1 column vector. It's elements are the second time derivatives of the degrees of freedom: three Euler angles and three linear coordinates:

$$\underline{X} = \langle \theta_1, \theta_2, \theta_3, X, Y, Z \rangle^T \tag{5}$$

The angles define the rotation between $\mathbf{e}^m$ and $\mathbf{e}^F$ and the linear coordinates define $\mathbf{r}_{Fm}$. Equation (4) is linear in the second derivatives of $\underline{X}$ and is very convenient for numerical time integration. Equation (4) stands for 6 scalar equations of motion for the rigid body having 6 degrees of freedom.

2 THE EXTERNAL LOADS

Three types of external loads are addressed in this work: reaction loads transferred to the body by the elastic elements (long beams) attaching it to the frame, damping loads due to squeeze-film effects and electrostatic loads used to excite mechanical motion of the body (actuation).

2.1 Elastic Reaction Loads

The body is attached to the rigid frame by long and thin beams. The scope of this work is restricted to the classical linear beams theory. Each element is modeled as a double-clamped beam numbered B_i. It's attachments to the body and to the frame are modeled by attachment points designated P_i and F_i respectively – see Figure 1. Via these points, the reaction torque $\mathbf{T}^{ri}$ and force $\mathbf{F}^{ri}$ are transmitted to the body. P_i and F_i are the origins of the systems of coordinates $\mathbf{e}^{Pi}$ and $\mathbf{e}^{Fi}$ respectively. While the angular orientation and the distance between these systems is known as initial conditions, they are calculated for each integration step. The orientation and distance between $\mathbf{e}^{Pi}$ and $\mathbf{e}^m$ is fixed because the body is rigid. The reaction torque and force, as a function of the relative displacements and angles between $\mathbf{e}^{Pi}$ and $\mathbf{e}^{Fi}$ are given by the classical matrix form [6]:

$$\underline{f} = \underline{K}\underline{\varepsilon} \tag{6}$$

Where $\underline{f}$ is a column vector of the 6 components of the reaction loads resolved in $\mathbf{e}^{Pi}$, $\underline{K}$ is the 6×6 stiffness matrix and $\underline{\varepsilon}$ is a column vector of the three angles and displacements. The elements of $\underline{K}$ are function of the beam's cross section dimensions, its length, and its material properties. Matrix $\underline{K}$ presents elastic coupling between the degrees of freedom. $\mathbf{r}_{cgpi}$ is the radius vector between cg and P_i thus, each reaction force $\mathbf{F}^{ri}$ is associated with reaction torque given by the vector product: $\mathbf{r}_{cgpi} \times \mathbf{F}^{ri}$. The resultant reaction loads in respect to cg are obtained by summing the reaction loads transmitted via each P_i.

2.2 Squeeze-Film Effect

In the general case, various damping mechanisms (linear and non-linear) can be modeled as equivalent damping loads transmitted to the body by N_d elements. In this work, only the squeeze film effect will be treated as it is the dominant mechanism in the microdevices under consideration. In these devices, the main body is performing a translation motion or angular motion relative to a rigid surface placed in a very narrow gap underneath. Thus appropriate model for the squeeze effect should be included. Analytical investigation of such mechanism referring to translation as well as angular motion was reported in [2]. In the present model, a resultant spring force and viscous-damping force are assumed to act on the center of mass of the body. The spring and damping coefficients are calculated by the above mentioned model and they are frequency dependant. These assumption coincides with the lumped model concept of this work.

2.3 Electrostatic Loads

The microdevices that are analyzed in this work are electrostaticaly actuated. A simple classic model of the electrostatic force between two parallel capacitor plates is being used for simplicity. The force is given by:

$$\underline{F}^{el} = \frac{\varepsilon A V^2}{2d^2} \tag{7}$$

Where ε is the dielectric constant of the material between the plates, A is the plates area, V is the potential difference between the plates and d is the nominal gap distance between them.

3 VERIFICATION OF THE MODEL

The theoretical derivation of the model and the numerical results were verified by comparison with

experimental results, analytical calculations and results from other simulation methods.

3.1 Comparison with Experimental Results

The motion of a torsion microresonator was measured by using external optical system. The microdevice is shown in Figure 2.

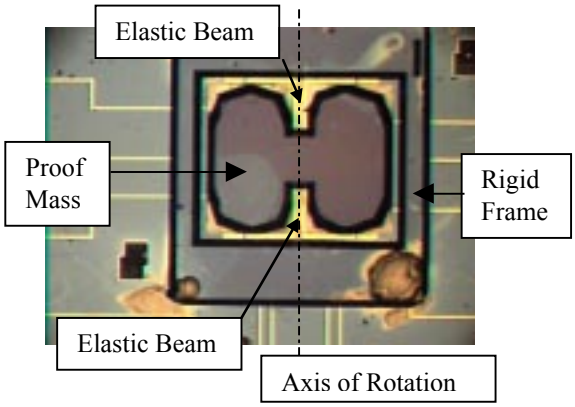

Figure 2: The torsion microresonator.

The bulk-micromachined H shaped is attached by two long beams to the rigid frame. The proof mass is suspended above an electrical chip and an air capacitor is created between them. By applying voltage to each side of the device an electrostatic force tilts it along the axis of rotation created by the twisted beams. To measure the motion a laser beam is pointed on the device face. The reflected beam is detected by a two-halves detector. The mechanical motion causes the reflected beam to sweep the detector thus the detector electrical output is a measure of the motion. The motion was created by applying a 20 Hz square wave of 45% duty cycle. Each wave applies an external shock to the device and its decaying motion can be seen in Figure 3a as measured under 10 mTorr pressure conditions. The simulation results are given in Figure 3b. These results show a normalized amplitude vs time because the measurement system characteristics – transferring the mechanical motion to electrical signal was not modeled. It can be seen that in both cases, an amplitude decay of 97% is obtained after 14 cycles and 0.008 seconds. Thus both simulation and measurement converge to the same damping ratio and natural frequency: 1750 Hz.

3.2 Comparison with Analytical Results

An analytical solution for the pull-in angle and voltage of torsion microactuator was presented by the authors [3]. The present model was used in successive runs applying increasing values voltage. The steady state tilt angle was obtained – till pull in occurred. In Table 1 the analytical calculations are compared with simulation results showing 1% deviation in the voltage and 6.4% deviation in angle.

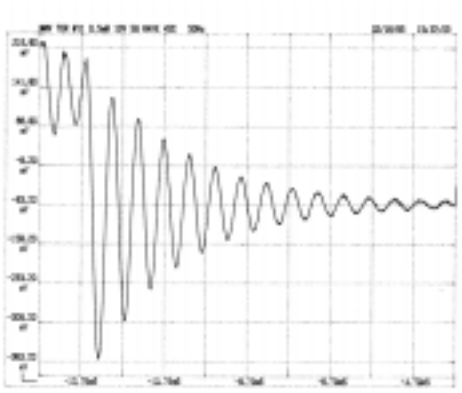

Figure 3a: Damped motion measurements.

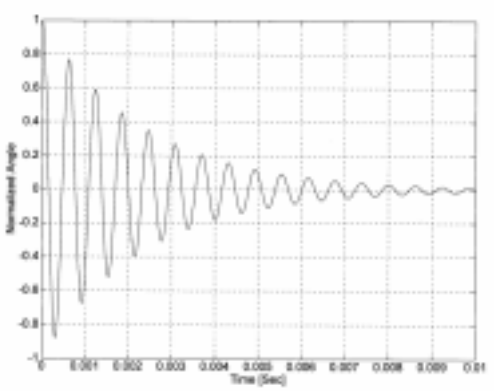

Figure 3b: Damped motion simulated.

	θ_{PI} [mrad]	V_{PI} [V]
Calculation	3.1	48
Simulation	2.9	47.5
Deviation %	6.4	1

Table 1: Comparison between calculated and simulated pull-in angel and voltage .

3.3 Comparison with more Experimental Results and Other Method of Simulation

In Figure 4 a micro spring-mass structure is shown with its system of coordinates. This structure consists of a proof mass and two long beams attaching it to a rigid frame. The motion of the proof mass is sensed by a novel optical method (MIDOS) based on alight source placed above the proof mass, and photodetectors placed on a chip underneath it. This method was discussed in details by the authors [7]. This microdevice was placed on a linear shaker creating mechanical white noise and thus it's natural frequencies were measured, as shown in Figure 5. The same system model was simulated by a commercial software, ADAMS, and by the current model to solve for the natural frequencies.

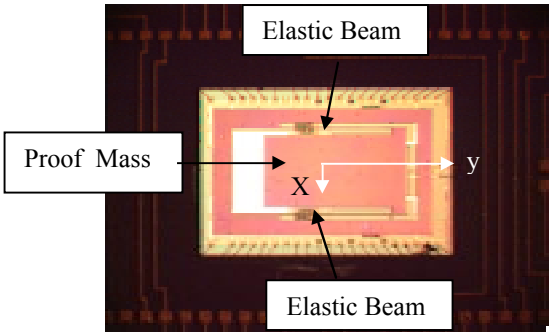

Figure 4: Micro-Mass-Spring Structure

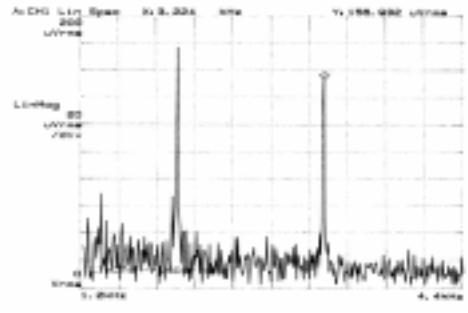

Figure 5: Natural frequencies measurements.

	ω_{nz} [KHz]	ω_{ny} [KHz]
Measured	1.992	3.224
ADAMS	2.212	3.218
Present Model	2.086	3.001

Table 2: Comparison between measured and simulated natural frequencies.

4 PARAMETRIC INVESTIGATION

The microdevice shown in Figure 4 can be used as a micro-gyro. When the proof mass is vibrating in perpendicular to the chip underneath, and an angular rate input vector is along the y axis, due to Coriolis effect, an output motion is excited along the x axis. As was shown by the authors [8], the sensitivity of the microgyro is highly dependant on its natural frequencies and thus governed by its geometrical properties. Of special interest is the influence of changes in the dimensions of the beams cross-section on the dynamical performance. In Figure 6 the dependency of the minimum detectable rate (MDR) on variations of the width of a rectangular beam cross section is shown. The MDR is normalized by the nominal value designed as working point. The plot is the result of a the full 6 degrees of freedom simulation.

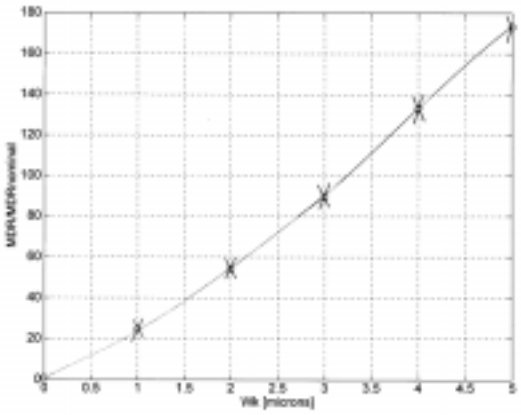

Figure 6: Minimum detectable rate vs beam cross section tolerances.

5 DESCUSSION

A lumped dynamical model, combined with appropriate models for external elastic loads, damping mechanisms and electrostatic loads, form a powerful tool for the early design phases of microdevices. The theoretical model was verified by comparison with experimental results , analytical calculations and simulations obtained by commercial software – showing good agreement. Finally, the verified model was used to perform parametric study showing its ability to predict the dependency of the dynamical performance of a microgyro on its dimensions.

REFERENCES

[1] Senturia S. D., "*CAD For Microelectromechanical Systems",* Int, Conf. Sol. Sta. Sens. Act., Transducers'95, Stockholm, June 26-29.

[2] Blech J.J., *"Squeeze Films",* Technion Report, Mechanical Engineering Department, EEC-111, March 1981.

[3] Degani O., Socher E., Lipson A., Leithner T., Seter D.J., Kaldor S., Nemirovsky Y.,*"Pull-In Study of an Electrostatic Torsion Microactuator",* J. Microelectromechanical Systems, Vol. 7, No. 4, pp.373-379, December 1998.

[4] Wittenburg J., *"Dynamics of Systems of Rigid Bodies",* B.G. Teubner Stuttgart, p. 19, 1977.

[5] Roberson R.E. & Shwertassek R.,*"Dynamics of Multibody Systems",* Springler-Verlag, p.47, 1988.

[6] Huston R.L.,*"Multibody Dynamics",* Butterworth-Heinemann, p.345, 1990.

[7] Degani O. Seter D.J., Socher E., Kaldor S., Nemirovsky Y.,*"Optimal Design and Noise Considerations of Micromachined Vibrating Rate Gyroscope with Modulated Integrative Optical Sensing",* J. Microelectromechanical Systems, Vol. 7, No.3, pp.329-338, September 1998.

[8] Seter D., Kaldor S., Scher E., Rosenberg J., Degani O., Nemirovsky Y.,*"Microelectromechanical Vibrating Inertial Sensors with integrative Optical Sensing",* Proc. Simposium Gyro Technology, p.10, 1998.